Since January 2020 Elsevier has created a COVID-19 resource centre with free information in English and Mandarin on the novel coronavirus COVID-19. The COVID-19 resource centre is hosted on Elsevier Connect, the company's public news and information website.

Journal of the Indian Chemical Society 99 (2022) 100640

Contents lists available at ScienceDirect

Journal of the Indian Chemical Society

journal homepage: www.journals.elsevier.com/journal-of-the-indian-chemical-society

The role of herbal plants in the inhibition of SARS-CoV-2 main protease: A computational approach

Ambrish Kumar Srivastava [a], Abhishek Kumar [b,c,*], Harshita Srivastava [a], Neeraj Misra [b]

[a] Department of Physics, Deen Dayal Upadhyaya Gorakhpur University, Civil Lines, Gorakhpur, 273009, Uttar Pradesh, India
[b] Department of Physics, University of Lucknow, University Road, Lucknow, 226007, Uttar Pradesh, India
[c] Department of Geology, Babasaheb Bhimrao Ambedkar University, (A Central University Vidya Vihar, Raebareli Road, Lucknow, 226025, Uttar Pradesh, India

ARTICLE INFO

Keywords:
COVID-19
SARS-CoV-2 M^{pro} inhibitors
Herbal plants
Natural extracts
DFT
Molecular dynamics

ABSTRACT

COVID-19 has quickly spread across the globe, becoming a pandemic. This disease has a variable impact in different countries depending on their cultural norms, mitigation efforts and health infrastructure. This study aims to assess the herbal plants in the pursuit of potential SARS-CoV-2 M^{pro} inhibitors using *in silico* approaches. We have considered 16 extracted compounds of 10 different species of these plants. In order to explain their inhibition properties and chemical reactivity pattern, we have performed the density functional theory based calculations of frontier molecular orbitals, molecular electrostatic potential surface and chemical reactivity descriptors. Our calculated lipophilicity, aqueous solubility and binding affinity of the extracted compounds suggest that the inhibition potentials in the order; harsingar > aloe vera > giloy > turmeric > neem > ginger > red onion > tulsi > cannabis > black pepper. On comparing the binding affinity with hydroxychloroquine, we note that the inhibition potentials of the extracts of harsingar, aloe vera and giloy are very promising. In order to validate this, we have also performed MD simulation and MM-PBSA binding free energy analysis. Therefore, we believe that these findings will open further possibilities and accelerate the works towards finding an antidote for this malady.

1. Introduction

The coronavirus disease (COVID-19) has been declared as a worldwide epidemic by the world health organization (WHO). This novel coronavirus was detected in late December 2019 and recognized in early January 2020 in China [1,2]. On 11 February 2020, the international committee on taxonomy of viruses declared this "severe acute respiratory syndrome coronavirus 2" (SARS-CoV-2) as the new virus [3]. Presumably, this virus picks up its name from the virus responsible for the SARS outbreak of 2003 as they are genetically related but different. Subsequently, the WHO announced "COVID-19" as the name of this new disease. The COVID-19 spread abruptly across the globe, becoming a pandemic within a couple of weeks and apart from China, the news of the carnage started pouring in from countries like the USA, Italy, Spain, France, Germany and Iran along with India on a day to day basis. Unfortunately, there has been no noticeable breakthrough in the management of this disease to date and the patient is given a treatment based on his observable and diagnosable symptoms. Although several attempts have been made in the research and development of the diagnostics, therapeutics and vaccines for this novel coronavirus [4], there exists no chemotherapeutic agent so far which has been shown unequivocally to be effective in treating human diseases due to a minuscule virus. To combat this deadly COVID-19, a number of conventional drugs like chloroquine, hydroxychloroquine, remdesivir, etc. have been tried and found with certain curative effect *in vitro* [5–7]. However, the clinical drug response is not very encouraging and toxicity remains an inevitable issue causing serious adverse effects. This prompted us to study the inhibition of SARS-CoV-2 main protease (M^{pro}) by herbal plants. Because of the inherent side effects of the synthetic chemicals used in allopathic drugs, a sizeable population has switched over to the traditional system of medicine (herbal medicine) for their primary health care. Ayurveda, the age-old Indian system of medicine, is increasingly becoming a sought after system to bank on. The ayurvedic treatment has become an alternative to conventional medicines due to several reasons including easy availability, less or no side effects and less cost. Therefore, in the present work, we have chosen a multitude of herbal plants such as harsingar (*Nyctanthes arbor-tristis*), giloy (*Tinospora cordifolia*), aloe vera (*Aloe barbadensis miller*), turmeric (*Curcuma longa*), neem (*Azadirachta indica*),

* Corresponding author. Department of Physics, University of Lucknow, University Road, Lucknow, 226007, Uttar Pradesh, India.
E-mail address: abhishekphy91@gmail.com (A. Kumar).

https://doi.org/10.1016/j.jics.2022.100640
Received 19 March 2022; Received in revised form 24 June 2022; Accepted 8 July 2022
Available online 13 July 2022

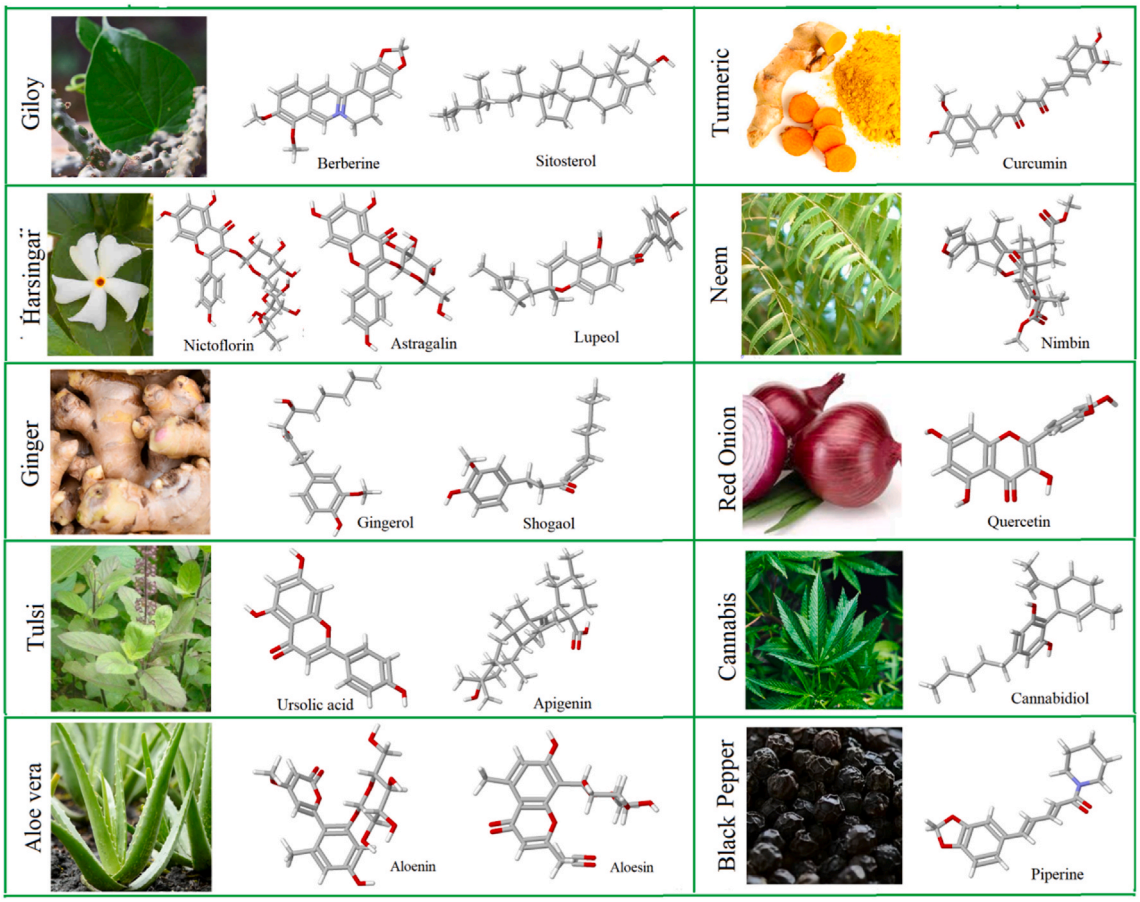

Fig. 1. Molecular structures of the compounds extracted from herbal plants. Harsingar (night jasmine or parijat) is distributed widely in sub-Himalayan regions, southwards to Godavari and also found in gardens as ornamental plant. Giloy (moonseed plant or guduchi) is a large deciduous, extensively spreading climbing shrub found throughout India and also in Bangladesh, Srilanka and China. Aloe vera (ghrit kumari) is a well known medicinal plant with sharp pointed, lanced shaped and edged leaves having its origin in African content, Turmeric (circumin or haldi), a traditional Chinese medicine, is commonly used species in Indian subcontinent, not only for health but also for the preservation of food. Neem (margosa tree) also called as Indian lilac with its centre of origin in southern and southeastern Asia, is regarded as 'village dispensary' in India and also a religious gift from nature. Red onion is a versatile vegetable, i.e., consumed fresh as well as in the form of processed products. Tulsi is the one of the most religious and medicinal plant in India and grown throughout the country from Andaman and Nicobar island to the Himalayas. Cannabis is a plant of psychoactive drug and black pepper is a kind of household species used in India. (For interpretation of the references to color in this figure legend, the reader is referred to the Web version of this article.)

ginger (*Zingiber officinale*), red onion (*Allium cepa*), tulsi (*Ocimum sanctum*), cannabis (*Cannabis sativa*) and black pepper (*Piper nigrum*). The pharmacological importance of these plants is well documented in the literature [8–10].

Given the importance and the urge of the discovery, in conjunction with the planning of new drugs, molecular modeling emerges as a powerful technique. This technique provides a set of tools to be used in the processes of identification, selection, optimization and characterization of new drug candidates due to its high capacity for forecasting and obtaining the structural and electronic properties of the complexes (receptor–ligand) analyzed [11,12]. In particular, computational techniques are recently found to be very useful in the study of inhibition of SARS-CoV-2 M^{pro} and a series of studies are already reported to identify more effective drug candidate against SARS-CoV-2 [13–22]. We have selected a few extracted compounds of these herbal plants and evaluated their inhibition properties against SARS-CoV-2 M^{pro} *in silico*. In order to obtain more insights, we have performed density functional theory based calculations as well. We have obtained encouraging responses from most of these medicinal plants, in general. The inhibition potentials of harsingar, aloe vera and giloy are particularly interesting. Therefore, we believe that this study should offer some insights into the development of alternative drugs for this novel coronavirus.

2. Methodology

Density functional theory (DFT) has been established as a powerful tool to study various aspects of biologically relevant molecules [23]. In the present study, the computational technique used incorporates DFT based B3LYP/6-311++G (d,p) scheme as implemented in GAUSSIAN 09 program [24]. This B3LYP method is a hybrid form of exchange-correlation functional which combines parameterized exchange term of A. D. Becke [25] and correlation term devised by Y. Lee, W. Yang and R. G. Parr [26]. The combination of hybrid functional B3LYP and triple-ζ basis set, in conjunction with the polarization functions (d, p), is a well-established basis set to obtained the unprecedented accuracy for the organic molecules under consideration [27]. The calculated global minimum energies, frontier molecular orbitals, molecular electrostatic potential surface, and global reactivity descriptors of the compounds (ligands) are useful to precisely understand the chemical reactions [28]. The ligand geometries have been optimized at ground state (in gas) without including any imaginary frequencies, and then used in molecular and quantum chemical calculation. Additionally, these geometries have been employed in docking analysis to achieve a significant stable ligand docked pose with receptor for the establishment of convincing intermolecular interactions in the respective complexes.

The electronic parameters [29,30] such as ionization potential (*I*),

Table 1
Calculated parameters of compounds extracted from herbal plants as possible inhibitors of SARS-CoV-2 M^{pro}.

Herbal plants	Extracted Compounds	Log *P*	Log *S*	Binding affinity (kcal/mol)	FF score	Active sites/ Binding residue (H-bond in Å)
Harsingar	Nictoflorin ($C_{27}H_{30}O_{15}$)	0.07	−2.29	−9.18	−2520	THR-190/ O–H (1.862) GLY-143/ N-H–O (2.311)
	Astragalin ($C_{21}H_{20}O_{11}$)	0.52	−2.45	−8.68	−1123	PHE-140/ O–H (2.197) GLU-166/ O–H (2.451)
	Lupeol ($C_{25}H_{26}O_4$)	5.12	−5.26	−8.28	−1160	THR-26/ N-H–O (2.027) THR-45/ O–H (2.187)
Aloevera	Aloenin ($C_{19}H_{22}O_{10}$)	0.05	−2.35	−9.13	−1120	PHE-140/ O–H (2.151)
	Aloesin ($C_{19}H_{22}O_9$)	0.12	−1.99	−8.79	−1135	GLY-143/ N-H–O (2.016) GLU-166/ N-H–O (2.297)
Giloy	Berberine ($C_{28}H_{18}NO_4$)	3.75	−4.16	−8.67	−1168	GLY-143/ N-H–O (2.540) GLY-143/ N-H–O (2.577)
	Sitosterol ($C_{29}H_{50}O$)	7.27	−7.35	−8.42	−1178	PHE-166/ O–H (2.080)
Turmeric	Curcumin ($C_{21}H_{20}O_6$)	3.62	−4.81	−8.44	−1196	GLY-143/ N-H–O (2.243)
Neem	Nimbin ($C_{30}H_{36}O_9$)	3.71	−4.36	−8.17	−1128	GLY-143/ N-H–O (2.161)
Ginger	Gingerol ($C_{17}H_{26}O_4$)	3.45	−3.57	−7.95	−1220	THR-190/ O–H (2.026)
	Shogaol ($C_{17}H_{24}O_3$)	4.95	−4.49	−7.86	−1209	GLY-143/ N-H–O (2.289) THR-26/ N-H–O (2.398) THR-24/ O–H (2.345)
Red Onion	Quercetin ($C_{15}H_{10}O_7$)	1.81	−3.06	−7.70	−1189	THR-26/ O–H (1.936) ASP-187/ O–H (2.756)
Tulsi	Ursolic acid ($C_{30}H_{48}O_3$)	6.35	−5.89	−7.46	−1152	GLY-143/ N-H–O (2.330)
	Apigenin ($C_{15}H_{10}O_5$)	3.07	−3.36	−7.38	−1210	THR-26/ O–H (1.994)
Cannabis	Cannabidiol ($C_{21}H_{30}O_2$)	6.10	−4.40	−7.10	−1214	
Black Pepper	Piperine ($C_{17}H_{19}NO_3$)	3.38	−3.28	−6.98	−1211	GLY-143/ N-H–O (2.325) THR-26/ N-H–O (2.529)

electron affinity (*A*), electronegativity (χ) and chemical hardness (η) of clusters have been calculated using the highest occupied molecular orbital (HOMO) and lowest unoccupied molecular orbital (LUMO) energies. These parameters can be calculated as below:

$$I = -E_{HOMO}$$

$$A = -E_{LUMO}$$

$$\chi = \tfrac{1}{2}(I + A)$$

$$\eta = \tfrac{1}{2}(I - A)$$

Where, E_{HOMO} and E_{LUMO} are the energies of HOMO and LUMO.

The molecular docking study was performed by the SwissDock web server [31,32] which incorporates an automated *in silico* molecular docking procedure based on the EADock ESS docking algorithm. To determine the inhibition properties of medicinal plants against SARS-CoV-2 main protease, the potential target protein was retrieved from the RCSB protein data bank (PDB ID: 6LU7) published in April 2020 [33,34]. The processed coordinates files for the ligands as well as SARS-CoV-2 M^{pro} (6LU7) has been uploaded, and docking was carried out with the 'Accurate' parameter option, which is considered to be the most extensive for the sampling of the binding modes. The output clusters have been obtained after each docking runs and classified based on the full fitness (FF) score by the SwissDock algorithm. A greater negative FF score suggests a more favorable binding mode between ligand and receptor with a better fit. The visual graphics of docking results have been generated by using the UCSF Chimera program [35].

In addition, we have calculated the lipophilicity (log *P*) and aqueous solubility (log *S*) using ALOGPS 2.1 program [36], which is based on the electro-topological state indices and associative neural network modeling [37]. These two parameters are very important for quantitative structure-property relationship (QSPR) studies.

3. Results and discussion

We have considered a total of 10 different varieties (species) of medicinal plants. Fig. 1 displays the molecular structures of a few (main) compounds extracted from these plants. We have focused on mainly those compounds which have been found to possess anti-malarial, antiviral or other similar activities. Nictoflorin ($C_{27}H_{30}O_{15}$), astragalin ($C_{21}H_{20}O_{11}$), lupeol ($C_{25}H_{26}O_4$) are extracted from the leaves of harsingar. Berberine ($C_{28}H_{18}NO_4$) and sitosterol ($C_{29}H_{50}O$) are chemical constituents of the stem of the giloy. Aloenin ($C_{19}H_{22}O_{10}$) and aloesin ($C_{19}H_{22}O_9$) are extracted from aloe vera leaves.

Curcumin ($C_{21}H_{20}O_6$) is extracted from the dried ground rhizome of the turmeric. Nimbin ($C_{30}H_{36}O_9$) is the first bitter compound isolated from the oil of neem. Gingerol ($C_{17}H_{26}O_4$) and shogaol ($C_{17}H_{24}O_3$) are two constituents of pungent ketones, which result in the strong aroma of ginger. Quercetin ($C_{15}H_{10}O_7$) is the main flavonoid content of (red) onion. Ursolic acid ($C_{30}H_{48}O_3$) and apigenin ($C_{15}H_{10}O_5$) are chemical constituents of tulsi leaves. Cannabidiol ($C_{21}H_{30}O_2$) major constituent of cannabis extracts and is devoid of the typical psychological effects of

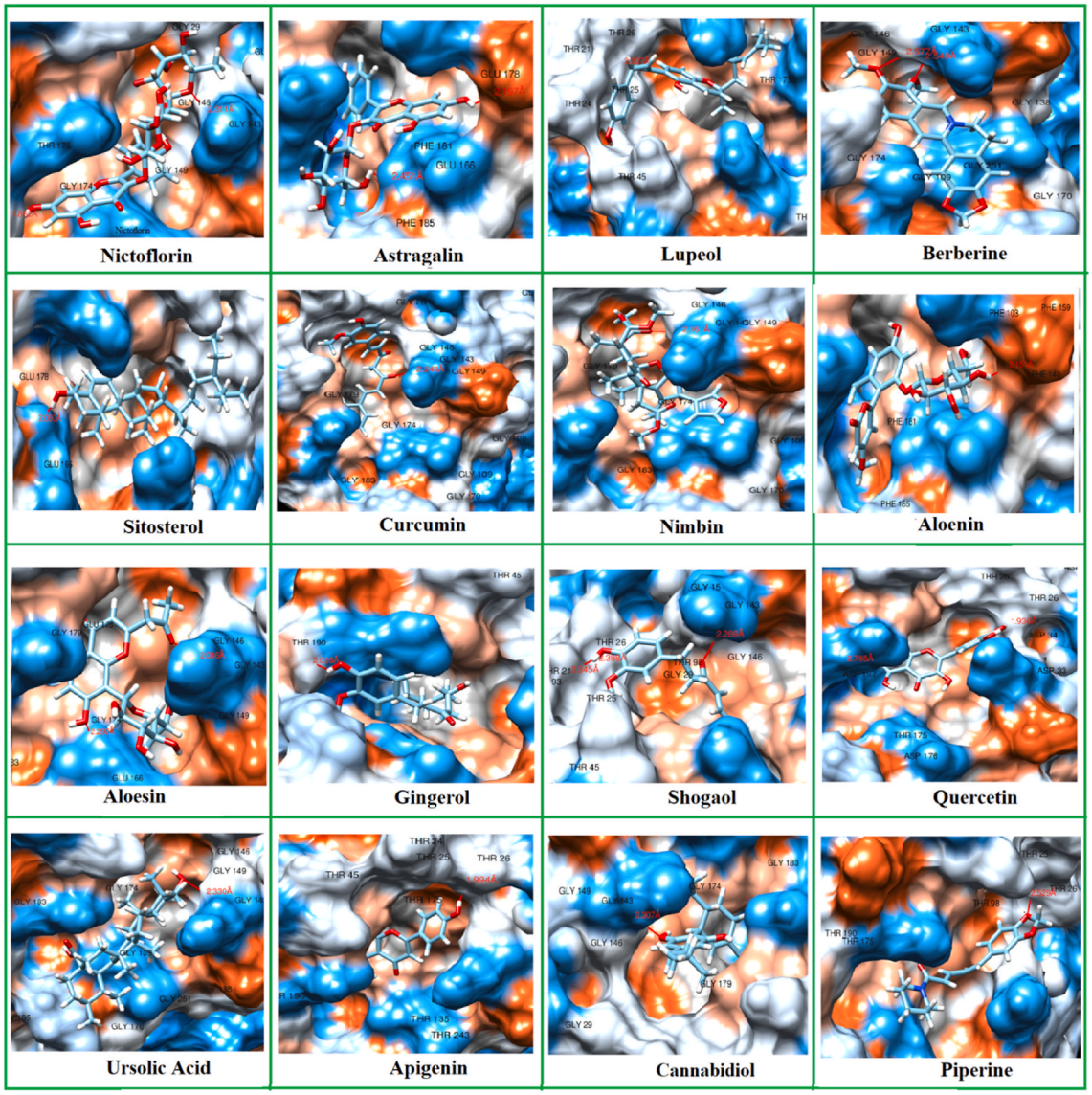

Fig. 2. The binding of SARS-CoV-2 M^{pro} (6LU7) receptor with the extracts of herbal plants explored by molecular docking.

cannabis in humans. Piperine ($C_{17}H_{19}NO_3$) is a naturally occurring alkaloid, which can be isolated from the plants of both the black and white pepper grains.

3.1. *Inhibition of SARS-CoV-2 M^{pro}*

3.1.1. *Pharmacological behavior*

In order to compare the biological activity and pharmacological behavior of the extracted compounds, we have evaluated their log *P* as well as log *S* values and listed in Table 1. Log *P* measures the hydrophilicity of a compound. The compounds having high log *P* values show poor absorption or low permeability. One can note that the log *P* values of most of these compounds lie in the range 2.64–4.95. These values indicate that the compounds can easily diffuse across the cell membranes due to their high organic (lipid) permeability. However, lupeol, sitosterol, ursolic acid and cannabidiol have log *P* in the range 5.12–7.27 (exceeding to 5) and therefore, they possess high hydrophobicity and poor absorption. On the contrary, nictoflorin, astragalin, aloenin, aloesin and quercetin possess high absorption due to their log *P* in the range 0.05–1.81. Log *S* represents the aqueous solubility of the compound. It is an important factor, associated with the bioavailability of compounds. Most of these compounds have log *S* values higher than −5, except lupeol, sitosterol and ursolic acid. Note that the log *S* values of more than 85% of compounds (drugs) fall in the range between −1 and −5 [38]. This is consistent with their log *P* values as poor solubility implies poor absorption and hence, bioavailability. Thus, log *P* along with log *S* values of these compounds confirmed their permeability across cell membranes. In particular, the nictoflorin, astragalin, aloenin, aloesin and quercetin seem to be more biologically potent. These parameters are also associated with their interaction with receptors.

3.1.2. *Molecular docking*

The molecular docking studies explore the interaction mechanism between ligands and receptors. The interactions between a ligand and receptor play a crucial role in the field of drug discovery. The molecular docking calculations have been performed as blind, i.e., covered the entire protein surface, not any specific region of the protein as the binding pocket in order to avoid sampling bias. The docking parameters such as binding affinity, FF score, and H-bond, bond-length along with amino acids (residue) found in the binding site pockets (active site) of 6LU7 are listed in Table 1. The results of molecular docking are displayed in Fig. 2.

The binding affinity (ΔG) of (drug) compounds depends on the type of bonding (H-bond) that occurs with the active site of the protein. The

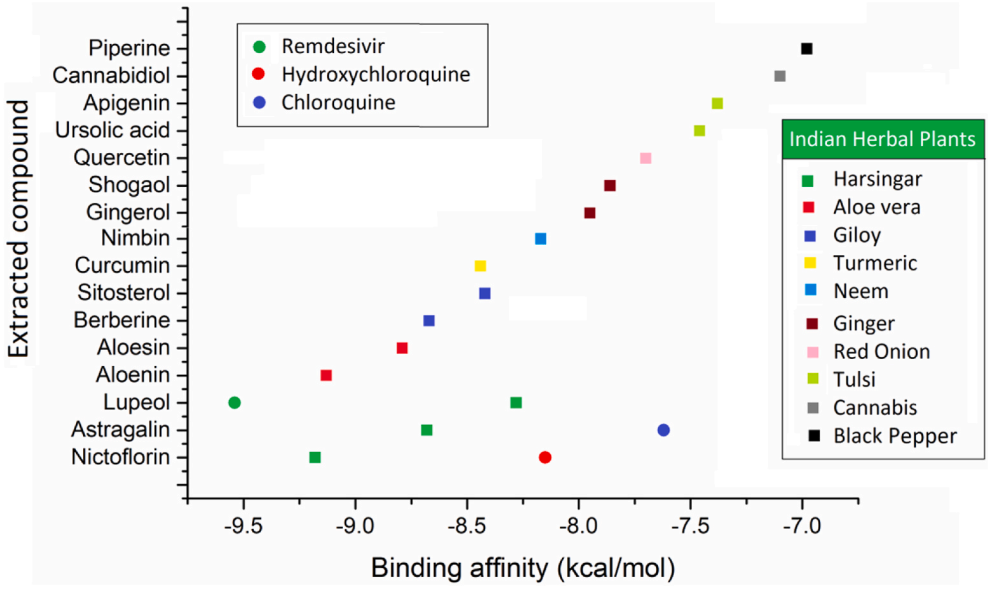

Fig. 3. Binding affinity plot of herbal plants and a few drugs for comparison of inhibition potential against SARS-CoV-2 M^{pro}.

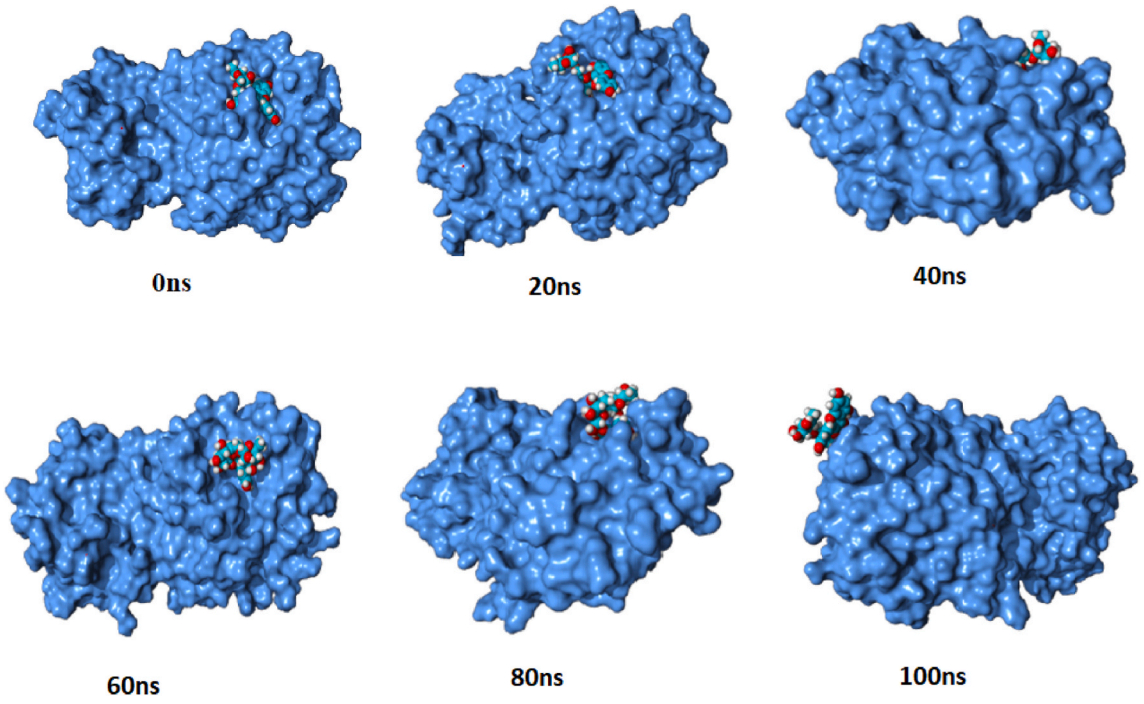

Fig. 4. The snapshots of nictoflorin-6LU7 complex at selected time interval during MD simulation.

results of docking show that the harsingar extracts nictoflorin, astragalin and lupeol form two H-bonds with different amino acids. Nictoflorin forms H-bonds of bond lengths 1.862 Å and 2.311 Å with the threonine (THR-26) and glycine (GLY-143) amino acids respectively. Astragalin forms H-bonds with phenylalanine (PHE-140) and glutamate (GLU-166) amino acids of bond lengths 2.197 Å and 2.451 Å respectively. Lupeol form two hydrogen bonds with same amino acid threonine (THR-26 & 45) with bond length 2.027 Å and 2.187 Å respectively. The compounds of aloe vera, aloenin forms H-bond (bond length = 2.151 Å) with phenylalanine (PHE-140) and aloesin forms two H-bonds with GLY-143 (bond length = 2.016 Å) and glutamate (GLU-166) with bond length = 2.297 Å. The constituents of giloy, berberine forms two H-bonds with the same amino acid GLY-143 having bond lengths of 2.540 Å and 2.577 Å, whereas sitosterol forms H-bond with PHE-166 of bond length 2.080 Å. The compounds of turmeric and neem, curcumin and nimbin form H-bonds with the same amino acid GLY-143 of bond lengths 2.243 Å and 2.161 Å, respectively. The compounds of ginger, gingerol forms H-bond with THR-190 (bond length = 2.026 Å) and shogaol forms three H-bonds, one with GLY-143 (bond length = 2.016 Å) and two with the THR-26 and THR-24 having bond lengths 2.398 Å and 2.345 Å, respectively.

The derivatives of red onion, quercetin form two H-bond with the polar amino acids THR-26 and ASP-187 of bond lengths 1.936 Å and 2.756 Å, respectively. The extracts of tulsi, ursolic acid and apigenin form H-bonds with the GLY-143 (bond length = 2.330 Å) and the THR-26 (bond length = 1.994 Å), respectively. The constituent of cannabis

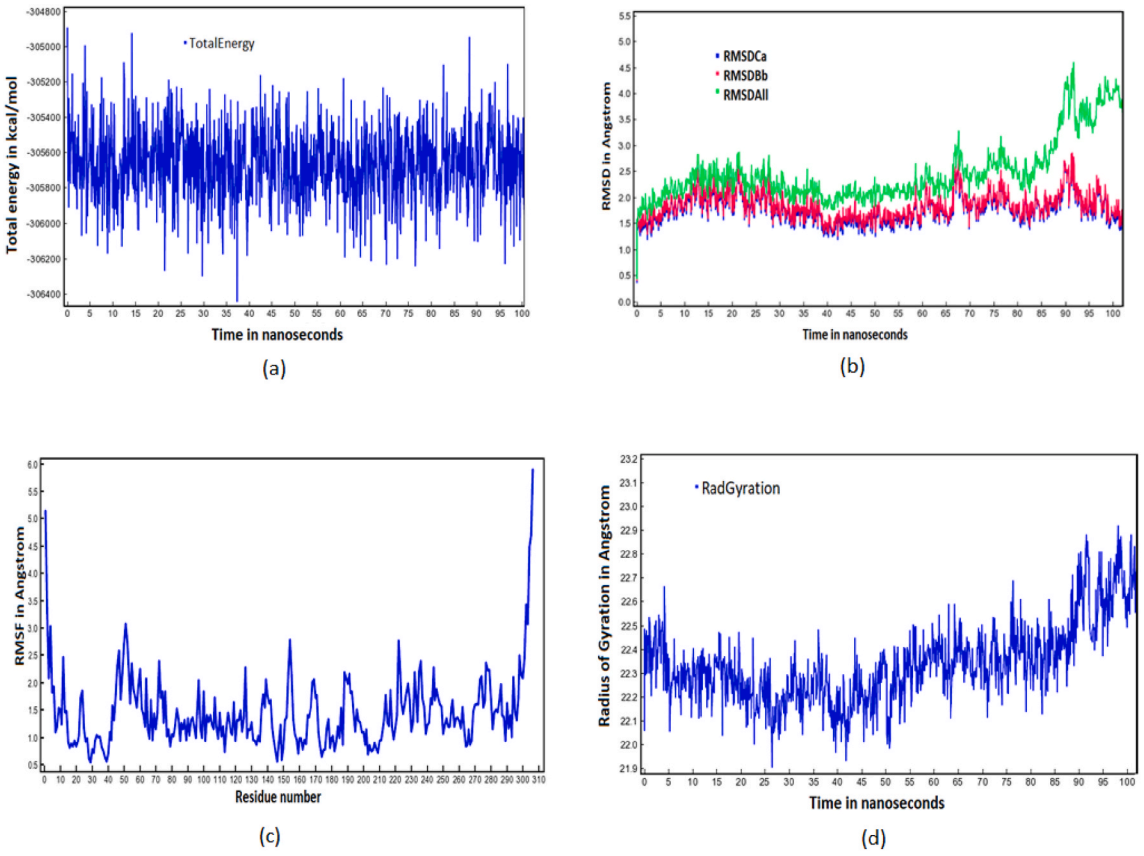

Fig. 5. The fluctuation in MD parameters during simulation; (a) total energy, (b) RMSD, (c) RMSF, and (d) radius of gyration.

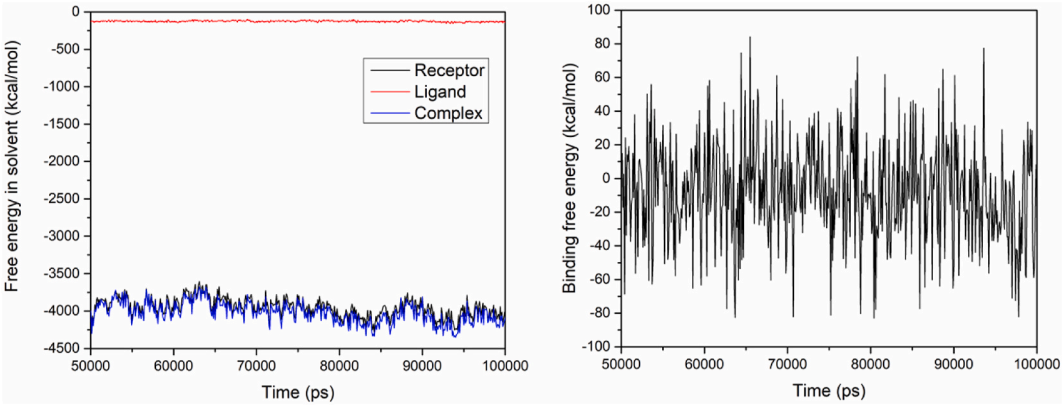

Fig. 6. MM-PBSA analysis of binding free energy of nictoflorin-6LU7 complex.

and black pepper, cannabidiol and piperine forms H-bond with the GLY-143 (bond length = 2.325 Å), a non-polar amino acid and THR-26 of bond lengths 2.243 Å a polar amino acid respectively.

Thus, our docking analyses suggest that the SARS-CoV-2 M^{pro} (6LU7) can be inhibited by the extracts of herbal plants. Based on the binding affinity, the inhibition potential of these plants (based on their extracts) can be ranked as; harsingar > aloe vera > giloy > turmeric > neem > ginger > red onion > tulsi > cannabis > black pepper. The highest inhibition potentials are obtained for the extracts of harsingar and aloe vera, namely, nictoflorin ($\Delta G = -9.18$) and aloenin ($\Delta G = -9.13$), respectively. This also provides us an opportunity to compare the ΔG value of the compounds extracted from other plants. Fig. 3 plots the binding affinities of these compounds, along with those of a few previously reported inhibitors such as remdesivir [5,6], chloroquine [5,7] and hydroxychloroquine [7].

Considering hydroxychloroquine as a reference, we note that the inhibition potentials of the extracts of harsingar, aloe vera and giloy are very encouraging. Further, the extracts of turmeric, neem, and ginger have larger inhibition potentials than that of chloroquine. The compounds extracted from other plants also possess certain inhibition properties against SARS-CoV-2 M^{pro}.

Experimentally, it has been found that the extracted compounds from the herbal plants having significant amount of total phenolic content (TPC) and total flavonoid content (TFC) possess promising antioxidant and anti-COVID-19 potentials [39]. In the present work, the studied compounds also belong to the phenolic and flavonoid family. Consequently, the outcomes of docking simulation are good evidence for anti-SARS-CoV-2 activity of these compounds. Previous reports also

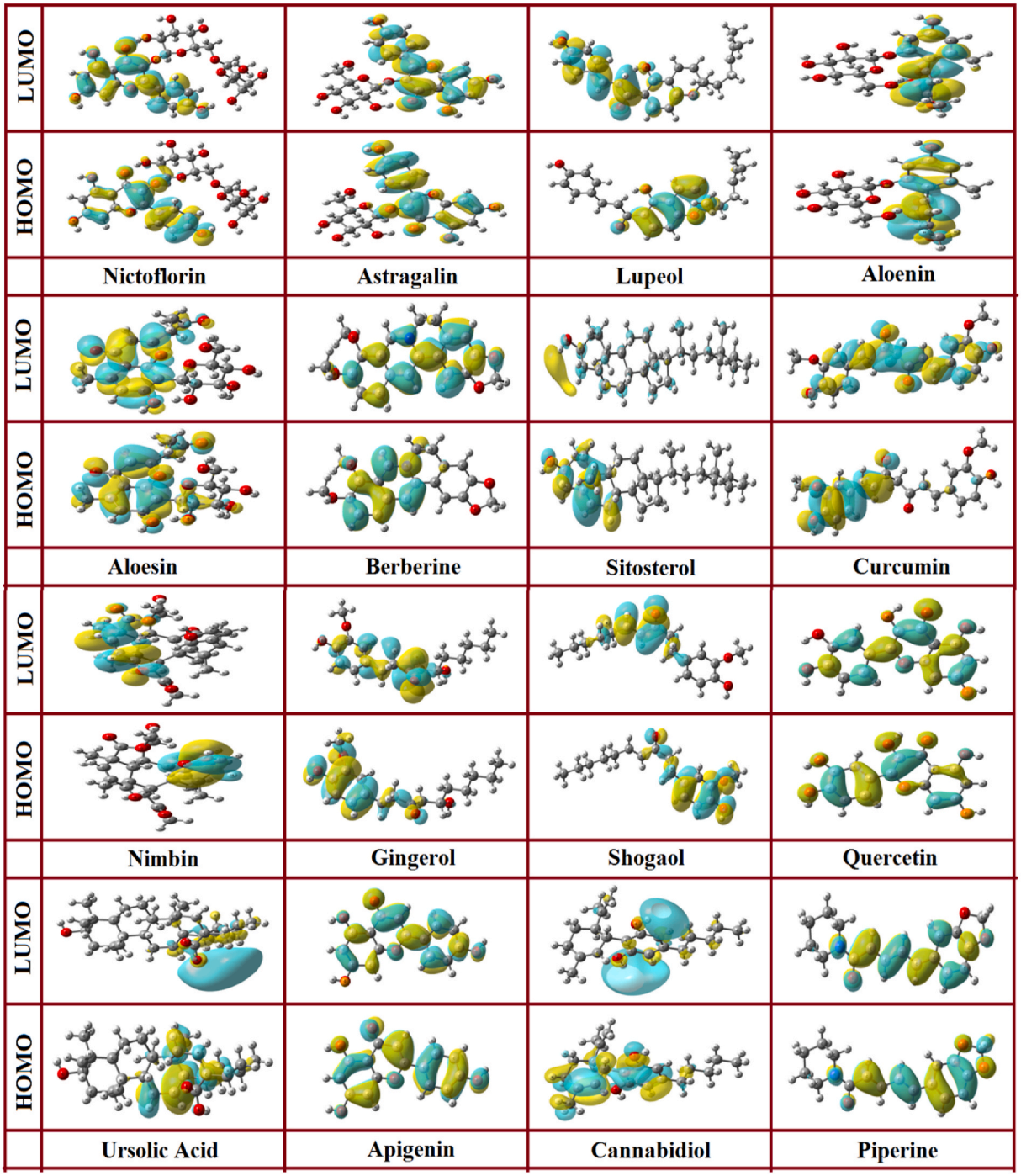

Fig. 7. Frontier molecular orbitals of extracts of herbal plants obtained at DFT-B3LYP/6-311++G(d,p) level.

showed that medicinal herbs or isolated constituents have inhibitory effect on various human corona virus strains [40,41]. The work reported by Balkrishna et al. also provides evidence in support of a tri-herbal formulation based on Ayurvedic system, that can effectively ameliorate the cytokine response mounted during SARS-CoV-2 infection [42]. Some previous reported results based on molecular dynamics simulation further supports the inhibitory potential of selected natural compounds against SARS-CoV-2 M^{pro} [43,44].

3.2. Molecular dynamics simulations

Molecular dynamics (MD) is extensively used computational program to investigate the stability of best pose complex obtained by docking. Therefore, we performed MD simulation by using the YASARA Structure [45] to analyze various properties of the receptor-ligand complex and to identify any predictable conformational swaps and interactivities with their structures over 100 nanoseconds (ns) with the speed of (2.5 fs time speed). The AMBER 14 force field was used for the simulation. The water molecules filled the simulation cell, which act as a solvent by default. The temperature is set at 298K and pressure control was disabled. The initial energy minimization process of each simulation was performed by the simulated annealing method, using the steepest gradient approach. The snapshot was taken at every 100ps and saved for further analysis.

Table 2
Calculated electronic parameters of compounds extracted from herbal plants as possible inhibitors of SARS-CoV-2 M^{pro}.

Extracted Compounds	I (eV)	A (eV)	E_g (eV)	χ (eV)	η (eV)
Nictoflorin ($C_{27}H_{30}O_{15}$)	5.96	1.93	4.03	3.94	2.01
Astragalin ($C_{21}H_{20}O_{11}$)	6.21	2.12	4.08	4.16	4.09
Lupeol ($C_{25}H_{26}O_4$)	5.85	2.35	3.50	4.10	1.75
Aloenin ($C_{19}H_{22}O_{10}$)	6.27	1.75	4.52	4.01	2.26
Aloesin ($C_{19}H_{22}O_9$)	6.94	1.93	5.00	4.43	2.50
Berberine ($C_{28}H_{18}NO_4$)	3.35	1.44	1.91	2.39	0.95
Sitosterol ($C_{29}H_{50}O$)	6.40	0.36	6.04	3.38	3.02
Curcumin ($C_{21}H_{20}O_6$)	6.19	2.43	3.76	4.31	1.88
Nimbin ($C_{30}H_{36}O_9$)	6.40	2.09	4.31	4.24	2.15
Gingerol ($C_{17}H_{26}O_4$)	6.25	1.06	5.20	3.65	2.59
Shogaol ($C_{17}H_{24}O_3$)	6.14	1.76	4.38	3.95	2.19
Quercetin ($C_{15}H_{10}O_7$)	5.76	1.96	3.80	3.86	1.90
Ursolic acid ($C_{30}H_{48}O_3$)	6.64	0.54	6.10	3.59	3.05
Apigenin ($C_{15}H_{10}O_5$)	6.25	1.84	4.41	4.04	2.20
Cannabidiol ($C_{21}H_{30}O_2$)	6.02	0.48	5.55	3.25	2.77
Piperine ($C_{17}H_{19}NO_3$)	5.72	2.04	3.67	3.88	1.84

3.2.1. MD trajectory analysis

We have considered the MD simulation of 6LU7 with nictoflorin as it possesses the highest binding affinity according to docking results (Table 1). The final snapshots at selected interval during MD simulation are shown in Fig. 4. One can see that the nictoflorin (ligand) is attached to the 6LU7 receptor during whole simulation time. The total energy, RMSD, RMSF and radius of gyration are plotted in Fig. 5 as a function of simulation time. The initial energy-minimization of the conformation at 0ns is −393614.032 kcal/mol. The calculated energy of the first snapshot at 100ps is 304895.861 kcal/mol, see Fig. 5(a). The total energy of the complex is constantly fluctuating in the period of 100 ns, with the lowest value of −306442.045 kcal/mol at 37.5 ns.

We have also analyzed the atomic root mean square deviations (RMSDs) of C_α atoms, backbone (Bb) and all-heavy atom (All) for 100 ns period in order to explore the structural stability of the complex. The graphical representation of RMSDs of C_α atoms, backbone (Bb) and all-heavy atom (All) is shown in Fig. 5(b). These RMSDs show a fluctuation from 1.3 Å to 2.8 Å 0 between ns to 40 ns and, consequently, the complex shows the stable behaviour. The lowest values of RMSD were acquired by C_α atoms. The value of RMSD for all-heavy atom (All) increases enormously, reaching up to 3.9 Å from 40 ns to 100 ns.

The root-mean-square fluctuation (RMSF) signifies the overall variation of every residue over the simulation time. Fig. 5(c) shows the RMSF plots of the complex. The observed RMSF values vary between 0.5 Å and 5.9 Å. The highest fluctuation shown by 300–310 residue number which reaches the RMSF value of 5.9 Å whereas the lowest RMSF fluctuation values between 0.5 Å-0.6 Å were acquired by 30–40 and 146-150 residue number. Further, the least fluctuation was noticed between residue numbers 80-130.

The compactness and stability of the protein structure is analyzed by the parameter known as radius of gyration (R_g), shown in Fig. 5(d). The lower value of R_g reveals that the system has better compactness and stability. The least fluctuation in R_g values has been noticed between 56 ns and 62 ns, which indicates the most favorable condition for the compactness and stability of the complex. Further, there is rapid increase in the value of R_g from 80 ns to 100 ns, which attains the highest value of 22.87 Å at 98.9 ns.

3.2.2. MM-PBSA binding free energy analysis

The molecular mechanics Poisson–Boltzmann surface area (MM-PBSA) method [52] was used to analyze the binding free energies of the 6LU7-nictroflorin complex trajectory obtained by the MD simulations with the macro scripts of YASARA structure. Considering the stability of the MD simulation, the simulation snapshots from the last 50 ns were employed at temperature, T = 298 K. The binding free energy of complex was calculated using the following equations:

$$\Delta G_{binding} = \Delta G_{complex} - [\Delta G_{ligand} + \Delta G_{receptor}]$$

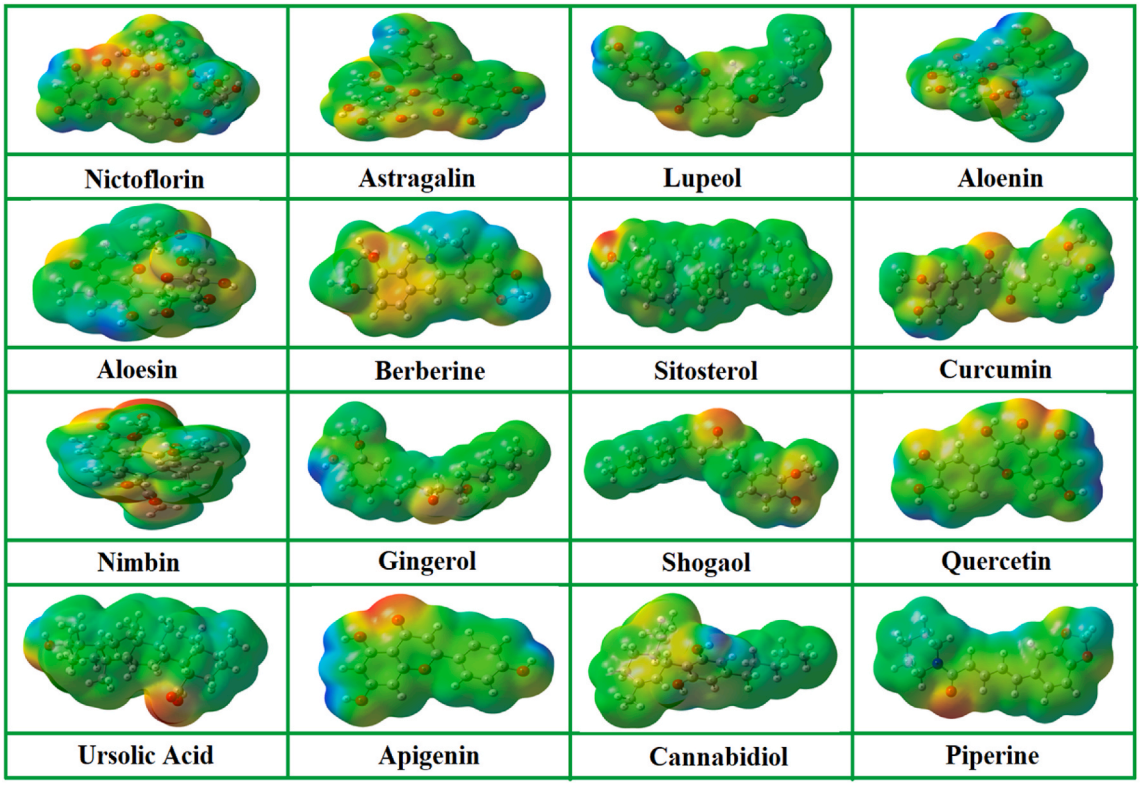

Fig. 8. The MESP plots of extracts of herbal plants obtained at DFT-B3LYP/6-311++G(d,p) level.

and

$$\Delta G_{binding} = \Delta G_{MM} + \Delta G_{PB} + \Delta G_{SA-T\Delta S} = (\Delta G_{elec} + \Delta G_{VdW}) + \Delta G_{PB} + \Delta G_{SA-T\Delta S}$$

where $\Delta G_{complex}$, ΔG_{ligand} and $\Delta G_{receptor}$ represent total free energy of respective species in solvent. The ΔG_{MM} is molecular mechanics interaction energy, which includes the electrostatic (ΔG_{elec}) and van der Waals interactions energies (ΔG_{VdW}). The ΔG_{PB} and ΔG_{SA} represent polar solvation and nonpolar solvation energy, respectively. TΔS is the contribution of entropy (S) to the free energy.

The total free energies of ligand (nictofluorin), receptor (6LU7) and 6LU7-nictoflorin complex as well as binding free energies (BFEs) of 6LU7-nictoflorin complex are plotted in Fig. 6 as a function of simulation time. From Fig. 6, the binding free energy is observed from −82.60 to 84.13 kcal/mol for the simulation time from 50 to 100 ns. Although the BFE values are not always negative, the average BFE is −8.34 kcal/mol, which indicates the successful binding of that the nictoflorin to 6LU7 receptor for most of the simulation time and in accordance with the binding affinity obtained by molecular docking studies.

3.3. DFT results

3.3.1. Frontier molecular orbitals analysis

The frontier molecular orbitals, such as HOMO and LUMO, play an important role in the chemical reaction of the compounds and their interactions with environment. The energy-difference between them is used to calculate the chemical reactivity, kinetic stability and hardness of the compound [46]. A compound having small HOMO-LUMO energy gap is generally classified with a high chemical reactivity and low kinetic stability, termed as soft molecule [47]. In this process, the reduction in energy gap indicates substantial intermolecular charge transfer within the molecule, which reflects the bioactivity of a molecule. Fig. 7 shows the HOMO and LUMO surfaces for natural compounds, where blue and yellow color distribution signify negative and positive phases of the frontier molecular orbitals' wavefunctions, respectively. Their energy gap (E_g) values are listed in Table 2. One can note that the E_g of all these compounds lie in the range 1.91–6.10 eV. The variation in their E_g results in the difference in the reactivity, and consequently, their inhibition potentials.

3.3.2. MESP plots

Molecular electrostatic potential (MESP) surface represents the distribution of electronic density on the surface of a molecular system. The MESP plot is an important map for predicting sites and relative reactivity for electrophilic attack in studies of biological recognition and interactions by hydrogen bonds. The electron density for each compound is represented by red regions (polar and negatively charged) and blue regions (non-polar and positively charged).

Fig. 8 shows the MESP plots of the studied compounds, in which the negative electrostatic potential (in red) represents the attraction of the proton by the region of high concentration of electrons in the molecule, whereas the positive electrostatic potential (in blue) corresponds to the repulsion of the proton by atomic nuclei [48]. One can see that a greater electron density is present around the oxygen atoms (O atom), thus representing the most likely locations for the occurrence of chemical interactions. This explains the presence of the O–H hydrogen bonds at the binding sites of SARS-CoV-2 M^{pro} receptor and ligands (see Table 1).

3.3.3. Chemical reactivity descriptors

The energy of HOMO and LUMO provides information about the ionization potential and electron affinity of a compound [49]. It has been reported that these values are mainly responsible for the biological interactions between ligands and proteins in a complex system [50–53]. Table 2 also lists some chemical reactivity descriptors for the compounds, extracted from herbal plants. It is observed that the compounds demonstrate a variation in their chemical reactivity pattern. For instance, the lower value of chemical hardness, being proportional to the energy gap, corresponds to soft molecules, i.e., more reactive molecules [54]. The maximum variation of these reactivity parameters have been seen in giloy extracted compounds, i.e., berberine and sitosterol. In order to explain the reactivity pattern, we take the extracted compounds of harsingar. From Table 1, we notice that the highest binding affinity of nictrofloroin (−9.18 eV) corresponds to O–H and N–H–O bonds with THR-190 and GLY-143 sites of SARS-CoV-2 M^{pro}, respectively. This is consistent with its lower electronegativity (3.96 eV), which causes the higher resistance to electron acceptance. Therefore, the O–H bond, in which nictoflorin has H-donor, becomes stronger than N–H–O bond. Likewise, the highest binding affinities, i.e., inhibition potentials of the extracted compounds from the aloe vera are also in accordance with their chemical reactivity descriptors.

4. Conclusions and perspectives

We have performed an *in silico* study on the inhibition of SARS-CoV-2 M^{pro} by the extracts of herbal plants. We noticed that all these plants possess inhibition properties to a certain extent. Based on the binding affinity as well as log *P* and log *S* values, harsingar, aloe vera and giloy appear as the most powerful inhibitors among the eleven plants considered here. Our MD simulation also validates this finding. Other potential inhibitors of SARS-CoV-2 M^{pro} include turmeric, neem and ginger. The inhibition potentials of all these plant extracts are found to be larger than those of chloroquine and hydroxychloroquine. Our DFT calculations on HOMO, LUMO and MESP surfaces along with some chemical reactivity descriptors provide further insights into inhibition properties of these compounds. These findings should be very interesting towards the development of alternative (herbal) medicines having no apparent side-effects.

Declaration of competing interest

The authors declare that they have no known competing financial interests or personal relationships that could have appeared to influence the work reported in this paper.

Acknowledgements

AKS acknowledges University Grants Commission (UGC), New Delhi, India for startup grant [30-466/2019(BSR)]. Authors are also thankful to Prof. S. N. Tiwari for useful discussions.

Appendix A. Supplementary data

Supplementary data to this article can be found online at https://doi.org/10.1016/j.jics.2022.100640.

References

[1] P. Zhou, X.L. Yang, X.G. Wang, B. Hu, L. Zhang, W. Zhang, H.R. Si, Y. Zhu, B. Li, C. L. Huang, H.D. Chen, A pneumonia outbreak associated with a new coronavirus of probable bat origin, Nature 579 (2020) 270–273.
[2] F. Wu, S. Zhao, B. Yu, Y.M. Chen, W. Wang, Z.G. Song, Y. Hu, Z.W. Tao, J.H. Tian, Y.Y. Pei, M.L. Yuan, A new coronavirus associated with human respiratory disease in China, Nature 579 (2020), 265-4.
[3] A.E. Gorbalenya, S.C. Baker, R. Baric, R.J.D. Groot, C. Drosten, A.A. Gulyaeva, B. L. Haagmans, C. Lauber, A.M. Leontovich, B.W. Neuman, D. Penzar, Coronaviridae Study Group of the International Committee on Taxonomy of Viruses. The species severe acute respiratory syndrome-related coronavirus: classifying 2019-nCoV and naming it SARS-CoV-2, Nat. Microbiol. 5 (2020) 536–538.
[4] G. Li, E. De Clercq, Therapeutic options for the 2019 novel coronavirus (2019-nCoV), Nat. Rev. Drug Discov. 19 (2020), 149-1.
[5] M. Wang, R. Cao, L. Zhang, X. Yang, J. Liu, M. Xu, Z. Shi, Z. Hu, W. Zhong, G. Xiao, Remdesivir and chloroquine effectively inhibit the recently emerged novel coronavirus (2019-nCoV) in vitro, Cell Res. 30 (2020), 269-12.
[6] T.P. Sheahan, A.C. Sims, S.R. Leist, A. Schäfer, J. Won, A.J. Brown, S. A. Montgomery, A. Hogg, D. Babusis, M.O. Clarke, J.E. Spahn, Comparative

therapeutic efficacy of remdesivir and combination lopinavir, ritonavir, and interferon beta against MERS-CoV, Nat. Commun. 11 (2020) 1–14.
[7] J. Liu, R. Cao, M. Xu, X. Wang, H. Zhang, H. Hu, Y. Li, Z. Hu, W. Zhong, M. Wang, Hydroxychloroquine, a less toxic derivative of chloroquine, is effective in inhibiting SARS-CoV-2 infection in vitro, Cell Discov. 6 (2020) 1–4.
[8] K. Mohanraj, B.S. Karthikeyan, R.P. Vivek-Ananth, R.B. Chand, S.R. Aparna, P. Mangalapandi, A. Samal, IMPPAT: a curated database of Indian Medicinal Plants, Phytochem. Therap. Sci. Rep. 8 (2018), 4329-17.
[9] S.R. Perumal, P. Gopalakrishnakone, Current status of herbal and their future perspectives, Nat. Proc. 1308 (2007) 1–13, https://doi.org/10.1038/npre.2007.1176.1, 1-1.
[10] C.P. Khare, Indian Medicinal Plants: an Illustrated Dictionary, Springer Science & Business Media, 2007.
[11] A. Kumar, A.K. Srivastava, S.K. Gangwar, N. Misra, G. Brahmachari, A. Mondal, S. Mondal, FT-IR, UV–visible, and NMR spectral analyses, molecular structure, and properties of Nevadensin revealed by density functional theory and molecular docking, Polycycl. Aromat. Comp. 40 (2020), 540-12.
[12] A.K. Srivastava, A. Kumar, S.K. Pandey, N. Misra, Spectroscopic analyses, intra-molecular interaction, chemical reactivity and molecular docking of imerubrine into bradykinin receptor, Med. Chem. Res. 25 (2016) 2832–2839.
[13] A. Ghaleb, A. Aouidate, H.B. El Ayouchia, M. Aarjane, H. Anane, S.E. Stiriba, In silico molecular investigations of pyridine N-Oxide compounds as potential inhibitors of SARS-CoV-2: 3D QSAR, molecular docking modeling, and ADMET screening, J. Biomol. Struct. Dyn. (2020) 1–11.
[14] Y. Wang, S. Murlidaran, D.A. Pearlman, Quantum simulations of SARS-CoV-2 main protease Mpro enable high-quality scoring of diverse ligands, J. Comput. Aided Mol. Des. 35 (2021) 963–968.
[15] G. Deganutti, F. Prischi, C.A. Reynolds, Supervised molecular dynamics for exploring the druggability of the SARS-CoV-2 spike protein, J. Comput. Aided Mol. Des. 35 (2) (2021), 195-12.
[16] A. Ghaleb, A. Aouidate, H.B. El Ayouchia, M. Aarjane, H. Anane, Salah-Eddine Stiriba, In silico molecular investigations of pyridine N-Oxide compounds as potential inhibitors of SARS-CoV-2: 3D QSAR, molecular docking modeling, and ADMET screening, J. Biomol. Struct. Dyn. (2020) 1–11.
[17] S. Beura, P. Chetti, In-silico strategies for probing chloroquine based inhibitors against SARS-CoV-2, J. Biomol. Struct. Dyn. (2020) 1–13.
[18] S. Shah, D. Chaple, S. Arora, S. Yende, C. Mehta, U. Nayak, Prospecting for Cressa cretica to treat COVID-19 via in silico molecular docking models of the SARS-CoV-2, J. Biomol. Struct. Dyn. (2021) 1–10.
[19] T.E. Tallei, Fatimawali, N.J. Niode, R. Idroes, B.M. Zidan, S. Mitra, I. Celik, F. Nainu, D. Ağagündüz, T.B. Emran, R.A. Capasso, Comprehensive review of the potential use of green tea polyphenols in the management of COVID-19, Evid. base Compl. Alternative Med. (2021) 1–13.
[20] S.S. Mousavi, A. Karami, T.M. Haghighi, S.G. Tumilaar, Fatimawali, R. Idroes, S. Mahmud, I. Celik, D. Ağagündüz, T.E. Tallei, T.B. Emran, R. Capasso, In silico evaluation ofn Iranian medicinal plant phytoconstituents as inhibitors against main protease and the receptor-binding domain of SARS-CoV-2, Molecules (2021) 5724.
[21] D. Ağagündüz, M.N. Çelik, M.E. Çıtar Dazıroğlu, R. Capasso, Emergent drug and nutrition interactions in COVID-19: a comprehensive narrative review, *Nutrients* (2021) 1550.
[22] S. Mahmud, G.K. Paul, M. Afroze, S. Islam, S.B.R. Gupt, M.H. Razu, S. Biswas, S. Zaman, M.S. Uddin, M. Khan, N.A. Cacciola, T.B. Emran, M.A. Saleh, R. Capasso, J. Simal-Gandara, Efficacy of phytochemicals derived from Avicennia officinalis for the management of COVID-19: a combined in silico and biochemical study, *Molecules* (2021) 2210.
[23] A.K. Srivastava, N. Misra, DFT Based Studies on Bioactive Molecules, Bentham Science Publishers Ltd. Singapore, 2021, https://doi.org/10.2174/9789814998369121010 1.
[24] W. Kohn, L.J. Sham, Self-consistent equations including exchange and correlation effects, Phys. Rev. 140 (1965) A1133.
[25] C. Lee, W. Yang, R.J. Parr, Development of the Colle-Salvetti correlation-energy formula into a functional of the electron density, Phys. Rev. B 37 (1988) 785.
[26] B. Miehlich, A. Savin, H. Stoll, H. Preuss, Results obtained with the correlation energy density functionals of Becke and Lee, Yang and Parr, Chem. Phys. Lett. 157 (1989) 200–206.
[27] W. Forner, W. Utz, Correlated ab initio and density functional calculations on small model molecules for the unit cell of polyparaphenylene in its aromatic and quinoidal forms: equilibrium geometries and vibrational spectra, J. Mol. Struct. 618 (2002), 65-19.
[28] Y. Zhao, D.G. Truhlar, Density functionals with broad applicability in chemistry, Acc. Chem. Res. 41 (2008), 157-10.
[29] R.G. Parr, R.G. Pearson, Absolute hardness: companion parameter to absolute electronegativity, J. Am. Chem. Soc. 105 (1983) 7512–7514.
[30] R.G. Parr, L.V. Szentpály, S. Liu, Electrophilicity index, J. Am. Chem. Soc. 121 (1999), 1922-2.
[31] A. Grosdidier, V. Zoete, O. Michielin, SwissDock, a protein-small molecule docking web service based on EADock DSS, Nucleic Acids Res. 39 (2011) W270–W277.
[32] A. Grosdidier, V. Zoete, O. Michielin, Fast docking using the CHARMM force field with EADock DSS, J. Comput. Chem. 32 (2011), 2149-10.
[33] Z. Jin, X. Du, Y. Xu, Y, et al., Structure of M pro from SARS-CoV-2 and discovery of its inhibitors, Nature 582 (2020), 289-4.
[34] http://www.rcsb.org/structure/6LU7.
[35] E.F. Pettersen, T.D. Goddard, C.C. Huang, G.S. Couch, D.M. Greenblatt, E.C. Meng, T.E. Ferrin, UCSF Chimera—a visualization system for exploratory research and analysis, J. Comput. Chem. 25 (2004) 1605–1607.
[36] J.J. Huuskonen, D.J. Livingstone, I.V. Tetko, Neural network modeling for estimation of partition coefficient based on atom-type electrotopological state indices, J. Chem. Inf. Comput. Sci. 40 (2000) 947–948.
[37] I.V. Tetko, V.Y. Tanchuk, T.N. Kasheva, A.E. Villa, Internet software for the calculation of the lipophilicity and aqueous solubility of chemical compounds, J. Chem. Inf. Comput. Sci. 41 (2001), 246-6.
[38] W.L. Jorgensen, E.M. Duffy, Prediction of drug solubility from structure, Adv. Drug Deliv. Rev. 54 (2002), 355-11.
[39] I.M. Imran, M. Khalid, M.S. Ullah, N. Khalid, M.A. Assiri, R. Thomas, S. Muthu, M. A.R. Basra, M. Hussein, A.G. Al-Sehemi, M. Shahzad, Phenolic and flavonoid contents in Malva sylvestris and exploration of active drugs as antioxidant and anti-COVID19 by quantum chemical and molecular docking studies, J. Saudi Chem. Soc. 25 (2021), 101277.
[40] Almasian, F. Najafi, M. Eftekhari, M.R.S. Ardekani, M. Sharifzadeh, M. Khanavi, Polyurethane/carboxymethylcellulose nanofibers containing malva sylvestris extract for healing diabetic wounds: preparation, characterization, in vitro and in vivo studies, *Mater. Sci. Eng.,* C 114 (2020), 111039.
[41] J. Bastida, R. Lavilla, F. Viladomat, Chemical and biological aspects of Narcissus alkaloids, Alkaloids - Chem. Biol. 63 (2006) 87–179.
[42] A. Balkrishna, S. Haldar, H. Singh, P. Roy, A. Varshney, Coronil, A tri-herbal formulation, attenuates spike-protein-mediated SARS-CoV-2 viral entry into human alveolar epithelial cells and pro- inflammatory cytokines production by inhibiting spike protein-ACE-2 interaction, J. Inflamm. Res. 14 (2021) 869–915.
[43] S. Bharadwaj, A. Dubey, U. Yadava, S.K. Mishra, S.G. Kang, V.D. Dwivedi, Exploration of natural compounds with anti-SARS-CoV-2 activity *via* inhibition of SARS-CoV-2 Mpro, Briefings Bioinf. (2021) 1–17.
[44] S. Bharadwaj, E.I. Azhar, M.A. Kamal, L.H. Bajrai, A. Dubey, K. Jha, U. Yadava, S. G. Kang, V.D. Dwivedi, SARS-CoV-2 Mpro inhibitors: identification of anti-SARS-CoV-2 Mpro compounds from FDA approved drugs, J. Biomol. Struct. Dyn. (2020), https://doi.org/10.1080/07391102.2020.1842807.
[45] E. Krieger, R.L. Dunbrack, R.W. Hooft, B. Krieger, Assignment of protonation states in proteins and ligands: combining pK a prediction with hydrogen bonding network optimization, in: M. Gore, U.B. Jagtap (Eds.), Computational Drug Discovery and Design, Methods in Molecular Biology, Springer Science+Business Media, New York, NY, 2012, pp. 405–421.
[46] R.G. Pearson, Electronic spectra and chemical reactivity, J. Am. Chem. Soc. 110 (1988) 2092–2095.
[47] K.S. Thanthiriwatte, K.M.N. de Silva, Non-linear optical properties of novel fluorenyl derivatives-ab initio quantum chemical calculations, J. Mol. Struct. 617 (2002), 169-6.
[48] I. Fleming, Frontier Orbitals and Organic Chemical Reactions, Wiley, Hoboken, NJ, USA, 1977.
[49] R.A. Costa, E.S.A. Junior, G.B.P. Lopes, et al., Structural, vibrational, UV–vis, quantum-chemical properties, molecular docking and anti-cancer activity study of annomontine and N-hydroxyannomontine β-carboline alkaloids: a combined experimental and DFT approach, J. Mol. Struct. 1171 (2018), 682-13.
[50] K.M. Honório, A.B.F. da Silva, An AM1 study on the electron-donating and electron-accepting character of biomolecules, Int. J. Quant. Chem. 95 (2003), 126-6.
[51] R.R. Da Silva, T.C. Ramalho, J.M. Santos, et al., On the limits of highest-occupied molecular orbital driven reactions: the frontier effective-for-reaction molecular orbital concept, J. Phys. Chem. 110 (2006), 1031-10.
[52] V.G. Maltarollo, D.C. Silva, K.M. Honório, Advanced QSAR studies on PPARδ ligands related to metabolic diseases, J. Braz. Chem. Soc. 23 (2012), 85-10.
[53] X. Pang, L. Zhou, M. Zhang M, et al., Two rules on the protein-ligand interaction, Open Conf. Proc. J. 3 (2012).
[54] R.A. Costa, K.M.T. Oliveira, Quantum chemical properties investigation and molecular docking analysis with DNA topoisomerase II of β-carboline indole alkaloids from Simaba guianensis: a combined experimental and theoretical DFT study, Struct. Chem. 29 (2018), 299-15.